Monthly Notices
of the
ROYAL ASTRONOMICAL SOCIETY

MNRAS **435,** 3017–3027 (2013) doi:10.1093/mnras/stt1496
Advance Access publication 2013 August 31

Large-scale analysis of the SDSS-III DR8 photometric luminous galaxies angular correlation function

Fernando de Simoni,[1,2]⋆ Flávia Sobreira,[2,3] Aurelio Carnero,[2,3] Ashley J. Ross,[4] Hugo O. Camacho,[2,5] Rogerio Rosenfeld,[2,6] Marcos Lima,[2,5] Luiz A. N. da Costa[2,3] and Marcio A. G. Maia[2,3]

[1]*Departamento de Física e Matemática, PURO/Universidade Federal Fluminense, Rua Recife s/n, Rio das Ostras, RJ 28890-000, Brazil*
[2]*Laboratório Interinstitucional de e-Astronomia – LIneA, Rua Gal. José Cristino 77, Rio de Janeiro, RJ 20921-400, Brazil*
[3]*Observatório Nacional, Rua Gal. José Cristino 77, Rio de Janeiro, RJ 20921-400, Brazil*
[4]*Institute of Cosmology and Gravitation, Dennis Sciama Building, University of Portsmouth, Portsmouth PO1 3FX, UK*
[5]*Departamento de Física Matemática, Instituto de Física, Universidade de São Paulo, São Paulo, SP CP 66318, CEP 05314-970, Brazil*
[6]*Instituto de Física Teórica and ICTP South American Institute for Fundamental Research, Universidade Estadual Paulista, Rua Dr. Bento T. Ferraz 271, São Paulo, SP 01140-070, Brazil*

Accepted 2013 August 7. Received 2013 August 2; in original form 2013 June 5

ABSTRACT

We analyse the large-scale angular correlation function (ACF) of the CMASS luminous galaxies (LGs), a photometric-redshift catalogue based on the Data Release 8 (DR8) of the Sloan Digital Sky Survey-III. This catalogue contains over 600 000 LGs in the range $0.45 \leq z \leq 0.65$, which was split into four redshift shells of constant width. First, we estimate the constraints on the redshift-space distortion (RSD) parameters $b\sigma_8$ and $f\sigma_8$, where b is the galaxy bias, f the growth rate and σ_8 is the normalization of the perturbations, finding that they vary appreciably among different redshift shells, in agreement with previous results using DR7 data. When assuming constant RSD parameters over the survey redshift range, we obtain $f\sigma_8 = 0.69 \pm 0.21$, which agrees at the 1.5σ level with Baryon Oscillation Spectroscopic Survey DR9 spectroscopic results. Next, we performed two cosmological analyses, where relevant parameters not fitted were kept fixed at their fiducial values. In the first analysis, we extracted the baryon acoustic oscillation peak position for the four redshift shells, and combined with the sound horizon scale from 7-year *Wilkinson Microwave Anisotropy Probe* (*WMAP*7) to produce the constraints $\Omega_m = 0.249 \pm 0.031$ and $w = -0.885 \pm 0.145$. In the second analysis, we used the ACF full shape information to constrain cosmology using real data for the first time, finding $\Omega_m = 0.280 \pm 0.022$ and $f_b = \Omega_b/\Omega_m = 0.211 \pm 0.026$. These results are in good agreement with *WMAP*7 findings, showing that the ACF can be efficiently applied to constrain cosmology in future photometric galaxy surveys.

Key words: surveys – cosmological parameters – large-scale structure of Universe.

1 INTRODUCTION

The study of the large-scale structure of the Universe represents an important cosmological tool and recent galaxy surveys have become sufficiently large to competitively constrain cosmological parameters. For instance, spectroscopy surveys such as the Two-degree Field Galaxy Redshift Survey (2dFGRS; Colless et al. 2001) and the Sloan Digital Sky Survey (SDSS; York et al. 2000) used the 3D galaxy clustering analysis to constrain cosmological parameters. Last year the WiggleZ (Parkinson et al. 2012) released its final cosmological results from galaxy distribution, measuring redshifts out to $z \sim 1$. The Baryon Oscillation Spectroscopic Survey (BOSS, Dawson et al. 2013), part of the SDSS-III, is an ongoing project that is pushing the analysis of the galaxy distribution to another level. It is going to measure more galaxies compared to previous spectroscopic surveys at an effective redshift of $z \sim 0.57$. Some few representative papers are Percival et al. (2007), Blake et al. (2011) and Anderson et al. (2013).

Some of the next generation galaxy surveys will be carried out with photometric data instead of spectroscopy, using broad-band photometry to estimate the so-called photometric redshifts, or photo-zs for short. These surveys will estimate photo-zs for a large number of objects, but with a lower accuracy compared to spectroscopic redshifts, effectively trading accuracy for statistical power. Obviously, this is only possible with a careful characterization of

⋆ E-mail: fsimoni@id.uff.br

the photo-z errors. The typical approach is to slice the survey into redshift shells with thickness of order of the photo-z errors, and study the angular clustering on each shell. The 3D information can then be partially restored by also including the correlations between different redshift shells and the photo-z errors.

One of the next large photometric surveys is the Dark Energy Survey (DES; The Dark Energy Survey Collaboration 2005), which had its first light in 2012 September. This survey expects to measure over $\sim$300 million galaxies within an area of 5000 $\deg^2$ of the southern sky up to redshift $z \sim 1.4$. Another proposed photometric galaxy survey is the Large Synoptic Survey Telescope (LSST) with expected science data for 2021 (Abate et al. 2012). This survey will detect over a billion galaxies and will go deeper than the DES in redshift.

Photometric galaxy surveys will demand a full understanding of the angular clustering of the galaxy distribution in order to provide useful cosmological information. Therefore several studies have been performed in order to gauge the use of the galaxy angular clustering at large scales, both on theoretical and observational grounds. We briefly review some of them below.

On the theoretical front, Simpson, Peacock & Simon (2009) performed the first study on the measurement of the baryon acoustic oscillation (BAO) peak in the galaxy angular correlation function (ACF) in configuration space using photometric redshifts. They emphasized the role of photo-z errors in establishing the connection between the observed BAO position and the sound horizon scale. Sobreira et al. (2011) forecasted the cosmological constraints in a DES like survey from the ACF full shape information using the Fisher matrix formalism. They found that DES will constrain the dark energy equation of state w with a precision of $\sim$20 per cent. Crocce, Cabré & Gaztañaga (2011a) verified the accuracy of the ACF theoretical covariance matrix against N-body simulations, showing that at scales larger than $\sim 20\,h^{-1}$ Mpc, the Gaussian covariance is a good approximation. Ross et al. (2011a) forecasted constraints on redshift-space distortion (RSD) parameters for a DES like survey from the ACF full shape information and Sánchez et al. (2011) developed a method to apply the BAO peak position in the ACF as a standard ruler, overcoming some issues outlined in Simpson et al. (2009).

On the observational front, only one galaxy survey had the characteristics to make it possible to look into the large-scale properties of the ACF using photo-zs: the SDSS. This survey produced a series of data releases with four of them leading to a cosmological analysis with photometric data: Data Release 3 (DR3; Finkbeiner et al. 2004); the DR4 which was used to produce the MegaZ photometric catalogue (Collister et al. 2007), the DR7 (Abazajian et al. 2009) and the recent DR8 luminous galaxies (LGs) catalogue (Ross et al. 2011b). These four photometric catalogues resulted in a series of results on the angular clustering of galaxies at large scales, mostly in the redshift range $0.45 \le z \le 0.65$.

Padmanabhan et al. (2007) estimated the angular power spectrum in eight redshift shells, constraining RSD parameters and $\Omega_{\rm m}$. Blake et al. (2007) used the MegaZ catalogue to produce the first cosmological constraints directly from the galaxy angular clustering using the angular power spectrum. Sawangwit et al. (2011) measured the large-scale ACF but did not constrain cosmological parameters due to an excess power at these scales. Thomas, Abdalla & Lahav (2010) produced a similar analysis as that of Blake et al. (2007), but for the improved DR7. Crocce et al. (2011b) used DR7 data to constrain the so-called RSD parameters with the ACF full shape information, but did not estimate the cosmology. Carnero et al. (2012) used the BAO peak position information in DR7 to find the sound horizon scale. Ross et al. (2011b) measured the large-scale ACF in DR8 in order to check the impact of systematics, reducing the excess of power at these scales reported earlier (Sawangwit et al. 2011; Thomas, Abdalla & Lahav 2011). Using the DR8, Ho et al. (2012) estimated the cosmological parameters from the full information of the angular power spectrum and Seo et al. (2012) found the sound horizon scale also from the angular power spectrum. Notice that the cosmological analysis in all of these studies was performed in harmonic space with the angular power spectrum, not in configuration space with the ACF full shape information.

In the present paper we focus on the less explored approach of using the full shape of the ACF in configuration space to derive constraints on cosmological parameters, following the steps outlined in Sobreira et al. (2011). We also estimate RSD parameters and define the BAO peak position using the method developed in Sánchez et al. (2011). For these purposes we measure the ACF with the SDSS-III DR8 photometric data, using the so-called CMASS LGs catalogue (Ross et al. 2011b).

This paper is organized as follows. In Section 2 we present the SDSS DR8 data to be analysed. In Section 3 we briefly describe the novel method to estimate the ACF introduced by Ross et al. (2011b) and discuss how to construct the full covariance matrix including correlation among redshift shells. For completeness, in Section 4 we describe the theoretical modelling of the ACF. In Section 5 we find the best-fitting RSD parameters, and compare to the values found by Crocce et al. (2011b) with a similar data set and also compare with BOSS DR9 spatial correlation function results (Reid et al. 2012). The cosmological analysis is finally performed in Section 6, where we apply two methods. First, we use the power law+Gaussian fit (PLG) approach first applied to real data by Carnero et al. (2012). Secondly, for the first time using real data, we perform an estimation of cosmological parameters from the full shape information in the ACF. Finally, Section 7 provides a summary and our conclusions.

Throughout this study, when not stated otherwise, we assume as fiducial cosmological model a flat Λcold dark matter (ΛCDM) universe with parameters as determined by 7-year *Wilkinson Microwave Anisotropy Probe* (*WMAP*7)[1] (Komatsu et al. 2011): dark matter density parameter $\Omega_{\rm cdm} = 0.222$, baryon density parameter $\Omega_{\rm b} = 0.0449$, Hubble parameter $h = 0.71$, primordial index of scalar perturbations $n_{\rm s} = 0.963$ and normalization of perturbations $\sigma_8 = 0.801$. All numerical codes developed for our analysis applied the GSL package,[2] and the linear matter power spectrum was computed with the CAMB package (Challinor & Lewis 2011).

2 THE DATA

2.1 Galaxy selection

In this work we use the imaging data from the SDSS DR8 (Aihara et al. 2011), which is publicly available by the SDSS team.[3] This photometric sample has the same selection as the BOSS targets,

[1] During the final stages of this paper the *WMAP*9 results were released (Hinshaw et al. 2012); as these results are similar to the previous *WMAP*7 ones we will continue to use the *WMAP*7 numbers since our findings would not be affected in a significant manner. Also, the Planck collaboration recently released its cosmological results (Ade et al. 2013); in this case it was found a significant difference with respect to *WMAP*7 mainly in $\Omega_{\rm m}$ and the Hubble parameter. We comment on the impact of this difference on our results along the paper.

[2] http://www.gnu.org/software/gsl/

[3] http://portal.nersc.gov/project/boss/galaxy/photoz/

Table 1. The four redshift shells used in this work. Columns show, for each shell, the photo-z range, the number of galaxies from Ho et al. (2012) and the mean photo-z dispersion from Ross et al. (2011b).

Redshift shell	N_{gal}	σ_{phot}
$0.45 \le z_{\mathrm{p}} \le 0.50$	154 531	0.043
$0.50 \le z_{\mathrm{p}} \le 0.55$	198 132	0.044
$0.55 \le z_{\mathrm{p}} \le 0.60$	190 603	0.052
$0.60 \le z_{\mathrm{p}} \le 0.65$	121 181	0.063

which was intended to have approximately constant stellar mass, the so-called CMASS (Ross et al. 2011b; White et al. 2011). The construction of this photometric catalogue is detailed in Ross et al. (2011b) and Ho et al. (2012), where special care was taken to identify and remove potential systematic errors that could affect the measurement of the angular clustering of galaxies.

With the appropriate selection and cuts, one ends up with a catalogue containing ~700 thousand galaxies, mostly in the photometric redshift range $0.45 \le z_{\mathrm{p}} \le 0.65$, which is going to be our limiting redshifts for the cosmological analysis. Following Ross et al. (2011b) we will call this sample luminous galaxies, or LGs for short. We split the data in the range $0.45 \le z_{\mathrm{p}} \le 0.65$ into four photo-z shells of width $\Delta z_{\mathrm{p}} = 0.05$ and measure the ACF for each shell. We note that these are the same shells used in Ross et al. (2011b), Ho et al. (2012), Seo et al. (2012) and de Putter et al. (2012).

2.2 Selection functions

The true redshift distribution is one of the most important and challenging quantities needed in order to produce trustable results when investigating the projected angular clustering of galaxies within a redshift shell. In this sense, it is as important as the ACF measurement itself. For the LGs sample used in this work, the photo-zs of the objects are fairly accurate. They were estimated with the neural network ANNZ code (Collister & Lahav 2004) using as training set 112 778 spectra, i.e. almost 10 per cent of the final photometric LGs sample. The photo-z dispersion and the number of galaxies in each of the four shells are displayed in Table 1.

The selection function convolves the redshift distribution with the photo-z errors and must be included in the ACF calculation as described in the next section. In Fig. 1 we reproduce the selection functions $\phi(z)$ for the four redshift shells estimated by Ross et al. (2011b), which is also publicly available. The selection functions overlap due to photo-z uncertainties, as expected. We properly account for this effect both in the ACF itself and in its covariance matrix, which accounts for the correlation amongst redshift shells, as explained in the next section. In order to speed up our numerical code to evaluate the theoretical ACF, we have smoothed the selection functions by applying a cubic spline, with an error below 0.01 per cent.

3 MEASURING THE ACF AND ESTIMATING ITS COVARIANCE

The estimation of the ACF was performed following Ross et al. (2011b). We use the 'A_{star}' method (see section 4.1 of Ross et al. 2011b) to correct for stellar density systematics and correct for the offset between SDSS photometry in the North and South Galactic

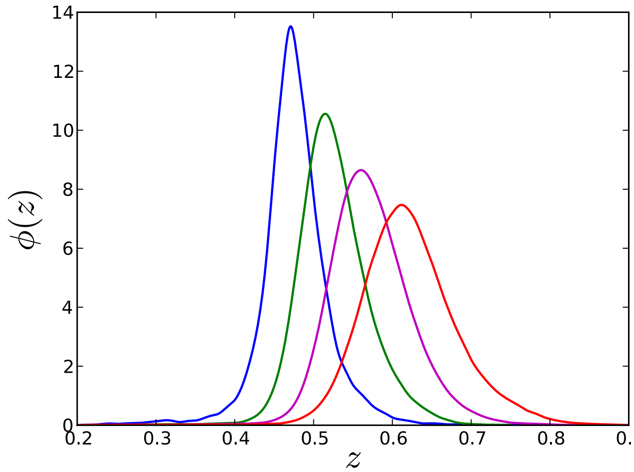

Figure 1. Selection functions for the set of redshift shells applied in the cosmological analysis (Ross et al. 2011b).

Cap (Schlafly & Finkbeiner 2011) using the method applied to obtain their 'Δ South' results. Below we outline the main features for this evaluation.

The catalogue is pixelized at $N_{\mathrm{side}} = 256$ using HEALPix (Gorski et al. 2005) and each pixel i is assigned a weight wt_i related to its overlap with the imaging footprint. The estimated ACF $\hat{\omega}(\theta)$ is obtained from

$$\hat{\omega}(\theta) = \frac{\sum_{ij} \delta_i \delta_j wt_i wt_j}{\sum_{ij} wt_i wt_j}, \tag{1}$$

where θ is the angular distance between pixel i and pixel j and the overdensity in pixel i, δ_i, is given by

$$\delta_i = \frac{n_i}{\bar{n} wt_i} - 1, \tag{2}$$

where n_i is the number of galaxies in pixel i and $\bar{n} = \sum n_i / \sum wt_i$.

In this work we measure the ACF in the angular range $1^\circ \le \theta \le 8^\circ$ with 35 angular bins for all redshift shells. This corresponds to spatial scales of $25 \lesssim r \lesssim 200\,h^{-1}$ Mpc. Note that in this approach, developed by Ross et al. (2011b) and Ho et al. (2012), it is straightforward to incorporate systematics effects, such as spurious clustering power due to extinction, seeing and star contaminations. In Fig. 2 we show the ACF measurements for the first and last redshift shells. They show no excess of power at large scales found previously by Thomas et al. (2011) and Sawangwit et al. (2011) and the BAO peak is apparent in both shells.

It is well known that the estimation of the covariance matrix for a galaxy clustering analysis in configuration space is a difficult task. The standard way to construct the covariance matrix $C(\theta_i, \theta_j)$, between angular bins i and j, is by the use of bootstrap methods, i.e. applying the data itself in the estimation. The most widely used approach is the so-called jackknife method. The idea is to divide the survey into N equal size areas, with the number of areas depending upon convergence tests, and producing the following errors (the covariance matrix is obtained with a similar procedure):

$$\sigma^2(\theta) = \frac{N-1}{N} \sum_{i=1}^{N} [\bar{\omega}(\theta) - \hat{\omega}_i(\theta)]^2, \tag{3}$$

where $\bar{\omega}(\theta)$ is the measured ACF for the full area and $\hat{\omega}_i(\theta)$ is the measurement when the ith jackknife region is removed. The main shortcoming is that the jackknife method may give unstable

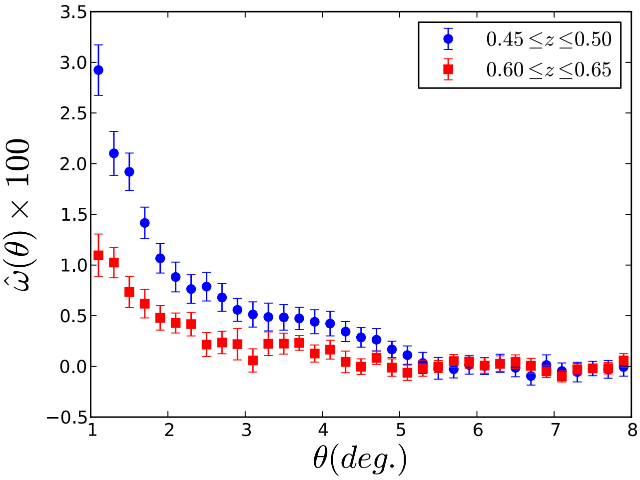

Figure 2. Estimated ACF for the first and last redshift shells. The error bars are estimated via jackknife method.

results, especially at large scales. A noisy covariance matrix can change the best-fitting value for the parameters in a pronounced manner. Moreover, it does not give the covariance between redshift shells, which is needed when analysing the full sample of galaxies. We illustrate the importance of including the covariance in the next section, where we compare results obtained using the full covariance and using only diagonal errors.

In a recent study, Crocce et al. (2011a) extensively studied a theoretical model for the ACF covariance matrix, assuming Gaussianity at large scale. They found that this approximation for the ACF covariance matrix at large scales is in very good agreement with the covariance from *N*-body simulations. This can be understood as a consequence of the central limit theorem, and of course, because at large scales one expects that the matter distribution follows a Gaussian distribution. Therefore, supported by this study, we will adopt the theoretical Gaussian covariance matrix in our analysis. As a bonus, for this covariance matrix it is straightforward to take into account correlation between redshift shells.

The full Gaussian covariance matrix is given by (for a detailed description see e.g. Crocce et al. 2011a; Sobreira et al. 2011)

$$C^{\alpha,\beta}(\theta_i,\theta_j) = \frac{2}{f_{\rm sky}} \sum_l \left[\frac{2l+1}{(4\pi)^2} P_l(\cos\theta_i) P_l(\cos\theta_j) \times \left(C_l^{\alpha,\beta} + 1/\bar{n}_\alpha\, \delta_{\alpha\beta} \right)^2 \right]. \quad (4)$$

The indices α and β label the redshift shells. The angular power spectrum given by

$$C_l^{\alpha,\beta} = \frac{2}{\pi} \int {\rm d}k\, k^2 P_{\rm m}(k) \Psi_l^{\alpha}(k) \Psi_l^{\beta}(k). \quad (5)$$

In the above equations $f_{\rm sky}$ is the fraction of the sky covered by the survey (in our case $f_{\rm sky} = 0.24$), P_l are Legendre polynomials, $\bar{n}_\alpha$ is mean density of galaxies in redshift shell α, $P_{\rm m}(k)$ is the matter power spectrum, $\Psi_l^{\alpha}(k)$ is the kernel function due to RSD for redshift shell α and $\delta_{\alpha\beta}$ is the Kronecker delta, showing that the shot-noise enters only in the autocovariance.

The cosmological parameters enter in the model for the covariance matrix through $P_{\rm m}(k)$ and the kernel $\Psi_l^{\alpha}(k)$. In an ideal analysis one should construct the likelihood $\mathcal{L}$ with this information added in the best-fitting search as was performed by Blake et al. (2007), i. e.

$$\mathcal{L} \propto |\mathbf{C}|^{-1/2} \exp\left(-\frac{\boldsymbol{d}^{\rm T} \mathbf{C}^{-1} \boldsymbol{d}}{2} \right), \quad (6)$$

where $\boldsymbol{d} = \hat{\boldsymbol{\omega}}(\theta) - \boldsymbol{\omega}(\theta)$ is the vector with the difference between the measured ACF and its theoretical value for all redshift shells. In our case, for four redshift shells we have $\hat{\boldsymbol{\omega}}(\theta) = (\hat{\omega}_1, \hat{\omega}_2, \hat{\omega}_3, \hat{\omega}_4)$, and $\mathbf{C}$ is the full covariance matrix with correlation between shells given in equation (4). It is well known that the covariance matrix $\mathbf{C}$ is nearly singular, $|\mathbf{C}| \approx 0$, and we apply the singular value decomposition method (Press, Flannery & Teukolsky 1986) in order to obtain its inverse.

Another problem when applying the full likelihood method is that it is very time consuming to evaluate the theoretical covariance matrix for a given set of parameters, rendering a Markov chain Monte Carlo (MCMC) estimation of the parameters not viable. In order to overcome this issue we adopt the following strategy. We first fix a cosmology, in our case *WMAP*7, and assign an initial constant value $b = 2$ for the bias, from which we generate a covariance matrix. Next we find the best-fitting value for the bias itself using the ACF full shape information as will be explained in the next section. In our case we find the following results for each redshift shell: $b = (1.94, 2.02, 2.15, 1.97)$.

With the fitted bias values, we compute the final covariance matrix that will be applied in our cosmological analysis. This approach assumes that most information in the covariance matrix comes from the bias or, in other words, most of the information in the covariance comes from the ACF amplitude and not its shape. In order to check the consistency of this assumption, we have compared the diagonal elements of the theoretical covariance matrix obtained using this procedure with the jackknife results estimated with equation (3) with $N = 20$. In Fig. 3 we show this comparison for the redshift shell $0.55 \le z_{\rm p} \le 0.60$. The results are in fair agreement, giving some confidence on the use of the theoretical covariance matrix. The consistency between the measured and theoretical covariance lead us to believe that our results would not change appreciably in a more complete analysis that vary the cosmology within the covariance matrix, or in a more conservative analysis that simply use the measured covariance.

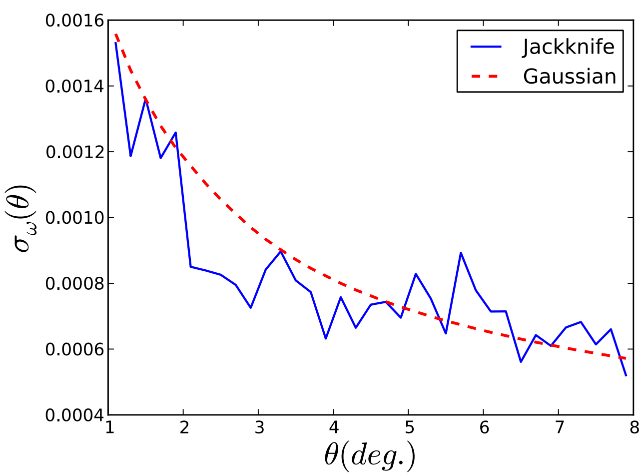

Figure 3. Comparison between jackknife and theoretical errors for the redshift shell $0.55 \le z_{\rm p} \le 0.60$.

Hence, we fix the cosmology when computing the covariance matrix, and we construct the standard χ^2 statistics,

$$-2\log\mathcal{L} = \chi^2 = \boldsymbol{d}^{\mathrm{T}}\mathbf{C}^{-1}\boldsymbol{d}, \tag{7}$$

to derive cosmological constraints from the data. This approach is widely applied in large-scale clustering analysis, such as the analysis performed in the BOSS DR9 data, e.g. Sánchez et al. (2012) and Anderson et al. (2012).

4 MODELLING THE ANGULAR CORRELATION FUNCTION

Our modelling of the ACF is based on the methods used in previous studies (see e.g. Crocce et al. 2011a; Ross et al. 2011a; Sobreira et al. 2011). The ACF is related to the two-point spatial correlation function $\xi^{(s)}$ in redshift space by

$$\omega(\theta) = \int_0^\infty \mathrm{d}z_1\,\Phi(z_1)\int_0^\infty \mathrm{d}z_2\,\Phi(z_2)\xi^{(s)}\left(r(z_1, z_2, \theta)\right). \tag{8}$$

The function $\Phi(z)$ is determined by the selection function of the survey $\phi(z)$, the dark matter to luminous bias factor $b(z)$ and the linear growth function $D(z)$ [normalized to $D(z=0)=1$] as $\Phi(z) = \phi(z)b(z)D(z)$. The comoving distance $r(z_1, z_2, \theta)$ between two galaxies at redshifts z_1 and z_2 separated by an angle θ and in a flat cosmology is given by the relation

$$r = \sqrt{\chi^2(z_1) + \chi^2(z_2) - 2\chi(z_1)\chi(z_2)\cos\theta}, \tag{9}$$

where $\chi(z_i)$ is the radial comoving distance of the object i to us (hereafter we use units with $c = 1$),

$$\chi(z) = \int_0^z \frac{\mathrm{d}z'}{H(z')}, \tag{10}$$

and $H(z)$ is the usual Hubble function.

The redshift-space spatial correlation function $\xi^{(s)}$, in the plane-parallel approximation, is given by (Hamilton 1992; Matsubara 2000)

$$\begin{aligned}\xi^{(s)}(r) = &\left[1 + \frac{1}{3}\left[\beta(z_1)+\beta(z_2)\right] + \frac{1}{5}\beta(z_1)\beta(z_2)\right]\xi_0(r)P_0(\mu) \\ &- \left[\frac{2}{3}\left[\beta(z_1)+\beta(z_2)\right] + \frac{4}{7}\beta(z_1)\beta(z_2)\right]\xi_2(r)P_2(\mu) \\ &+ \left[\frac{8}{35}\beta(z_1)\beta(z_2)\right]\xi_4(r)P_4(\mu).\end{aligned} \tag{11}$$

Here the $P_\ell(\mu)$ are the usual Legendre polynomials as a function of $\mu = \hat{d}\cdot\hat{r}$ (cosine of angle between the line of sight d and r) and $\beta(z) = f(z)/b(z)$ with $f(z) = \mathrm{d}\ln D/\mathrm{d}\ln a$. The correlation multipoles are related to the matter power spectrum $P_{\mathrm{m}}(k)$ through

$$\xi_l(r) = \frac{1}{2\pi^2}\int_0^\infty \mathrm{d}k k^2 P_{\mathrm{m}}(k) j_l(kr), \tag{12}$$

and can be written as (Hamilton 1992)

$$\xi_0(r) = \xi(r), \tag{13}$$

$$\xi_2(r) = \frac{3}{r^3}\int_0^r \mathrm{d}x\,\xi(x)\,x^2 - \xi(r), \tag{14}$$

$$\xi_4(r) = \xi(r) + \frac{5}{2}\left(\frac{3}{r^3}\int_0^r \mathrm{d}x\,\xi(x)\,x^2\right) - \frac{7}{2}\left(\frac{5}{r^5}\int_0^r \mathrm{d}x\,\xi(x)\,x^4\right), \tag{15}$$

where $\xi(r)$ is the real-space spatial correlation function. One can incorporate the effects of non-linearities using the so-called renormalized perturbation theory (RPT) approach (Crocce & Scoccimarro 2008), which determines the real-space correlation as

$$\xi_{\mathrm{nl}}(r) = \xi(r) + A_{\mathrm{mc}}\xi^{(1)}(r)\xi'(r), \tag{16}$$

where ξ' is the derivative of $\xi(r)$ with respect to r and

$$\xi^{(1)}(r) = \frac{1}{2\pi^2}\int_0^\infty \mathrm{d}k k P_{\mathrm{m}}(k) j_1(kr). \tag{17}$$

For A_{mc} we apply the value 1.55 found by Crocce et al. (2011a) from *N*-body simulations. Another non-linear effect that must be taken into account is the so-called Gaussian damping that affects mostly the BAO peak in the correlation function, and it is added phenomenologically by introducing a non-linear power spectrum $P_{\mathrm{NL}}(k)$ and substituting $P_{\mathrm{m}}(k)$ as (Crocce & Scoccimarro 2008)

$$P_{\mathrm{m}}(k) \to P_{\mathrm{NL}}(k) = P_{\mathrm{m}}(k)\exp\left[-r_{\mathrm{NL}}^2 k^2 D^2(z)/2\right], \tag{18}$$

with $r_{\mathrm{NL}} = 6.6\,\mathrm{Mpc}\,h^{-1}$. Crocce et al. (2011a) showed that this approach is in good agreement with simulations on scales above $\sim 20\,h^{-1}$ Mpc; therefore, our analysis will be applied above this scale.

In order to proceed it is worth pointing out some numerical issues that arise in going from $P(k)$ to $\xi(r)$. For this transformation, we have done some analysis varying the lower and upper limits in the integral (e.g. equation 12), since in principle it should be evaluated for all values of k. We found that with $k_{\mathrm{min}} \simeq 10^{-5}\,h\,\mathrm{Mpc}^{-1}$ and $k_{\mathrm{max}} \simeq 100\,h\,\mathrm{Mpc}^{-1}$, the integral converged and the time evaluation is reasonable for our purposes, something crucial for an extensive Markov chain analysis. Also, in order to compute the integrals in equations (14) and (15), we had to adopt a lower limit, and we found $r_{\mathrm{min}} \simeq 0.01\,h^{-1}$ Mpc to be a good value.

5 REDSHIFT-SPACE DISTORTION

We start by using the LG data to examine the constraints on the parameters describing RSD following closely the study by Crocce et al. (2011b).

In order to motivate the definition of the RSD parameters, we write the ACF in terms of a polynomial in the bias b and the velocity growth rate f:

$$\begin{aligned}\omega(\theta) = &\, b^2\omega_0(\theta) + bf\left(\frac{2}{3}\omega_0(\theta) + \frac{4}{3}\omega_2(\theta)\right) \\ &+ f^2\left(\frac{1}{5}\omega_0(\theta) + \frac{4}{7}\omega_2(\theta) + \frac{8}{35}\omega_4(\theta)\right),\end{aligned} \tag{19}$$

where $\omega_l(\theta)$ is the projection of the space correlation function multipoles in the redshift shell. This equation is in fact an approximation of equation (8), where one assumes that the functions $f(z)$, $D(z)$ and the bias do not evolve appreciably within each photo-z shell. We actually verified this assumption to hold in our case, by comparing both equations, (8) and (19), with our assumed cosmology and the LGs selection functions.

Since each term in equation (19) contains implicitly the product between σ_8^2 and $D(z)^2$, the two parameters that we are going to fit are

$$b(z)\sigma_8(z) = b\sigma_8 D(z) \tag{20}$$

and

$$f(z)\sigma_8(z) = f\sigma_8 D(z). \tag{21}$$

Table 2. Best-fitting values for RSD parameters for the three approaches: in the top part it is displayed the results allowing free parameters for each redshift shell; in the middle the velocity growth rate is assumed constant in all shells but allowing different $b(z)\sigma_8(z)$ for each shell and in the bottom part it is assumed constant $b(z)\sigma_8(z)$ and $f(z)\sigma_8(z)$ for all four shells.

Redshift shell	$b(z)\sigma_8(z)$	$f(z)\sigma_8(z)$
$0.45 \le z_p \le 0.50$	1.23 ± 0.06	0.66 ± 0.33
$0.50 \le z_p \le 0.55$	1.25 ± 0.11	0.26 ± 0.46
$0.55 \le z_p \le 0.60$	1.30 ± 0.06	0.93 ± 0.37
$0.60 \le z_p \le 0.65$	1.16 ± 0.08	1.11 ± 0.42
$0.45 \le z_p \le 0.50$	1.23 ± 0.05	
$0.50 \le z_p \le 0.55$	1.20 ± 0.05	0.72 ± 0.22
$0.55 \le z_p \le 0.60$	1.32 ± 0.05	
$0.60 \le z_p \le 0.65$	1.20 ± 0.07	
All shells	1.24 ± 0.04	0.69 ± 0.21

In order to compare with Crocce et al. (2011b), in this section we adopt the following values for the cosmological parameters in a flat ΛCDM Universe: $\Omega_m = 0.272$, $\Omega_b = 0.0456$, $n_s = 0.963$ and $h = 0.704$. We slice the survey into four redshift shells between $z_p = 0.45$ and 0.65 with constant width $\Delta z_p = 0.05$, as defined in Section 2.1.

We have constrained RSD parameters with three different approaches, all including correlations between shells due to photo-z dispersion. In the first approach we constrained $f\sigma_8$ and $b\sigma_8$ for each redshift shell, with a total of eight parameters. It should be noticed that within this approach the parameters best-fitting results are correlated. In the second approach we follow Padmanabhan et al. (2007), where it was noticed that the parameter $f\sigma_8$ does not change appreciably within the redshift limits in the ΛCDM model we adopt. Therefore, in this approach we fit only one $f\sigma_8$ parameter for all shells, but still allow $b\sigma_8$ to be different for each shell, for a total of five parameters to be fitted. In the third approach, we have assumed both $b\sigma_8$ and $f\sigma_8$ to be constant for all redshift shells, therefore, we have only two free parameters. This last approach is similar to what is done with spectroscopic survey analysis, which typically finds effective parameters over the whole survey range. The results for the three methods are respectively shown in Table 2.

The results for the first approach for the $b\sigma_8$ parameters are in good agreement with Crocce et al. (2011b), which reported $b\sigma_8 = 1.26$, 1.21 and 1.10 with 2 per cent error for the first three shells (they did not analyse our last shell), although we find somewhat larger errors of ∼5 per cent. If we assume $\sigma_8 = 0.8$, this translate to the following bias parameter for each shell: $b_1 = 1.94 \pm 0.08$, $b_2 = 2.02 \pm 0.08$, $b_3 = 2.15 \pm 0.08$ and $b_4 = 1.96 \pm 0.11$. Comparing with the results found by Ho et al. (2012) we see that the first three shells agree quite well, only the last shell is 10 per cent lower. Although in principle the angular power spectrum C_l and the ACF have the same information, in practice they can yield different results. This is mostly due to the need to include mask effects in the case of the angular spectra, and also in the estimation of the covariance matrix, which is nearly diagonal for the power spectrum. The two analyses, performed independently, are complementary and the consistency between them provides an interesting cross-check of systematics.

For the product of the growth rate with σ_8, Crocce et al. (2011b) found $f\sigma_8 = 1.14 \pm 0.57$, 0.024 ± 0.53 and 1.39 ± 0.46 in redshift shells similar to our three lowest. Within the large errors, the results are compatible. In Fig. 4, we show the best-fitting results for both parameters in each redshift shell. It shows that the first two shells are in agreement with the theoretical expectation within 1σ and the last two shells only agrees at the 2σ confidence level. For the bias parameters, it shows that only the third shell does not agree with a bias $b = 2$ at 1σ level.

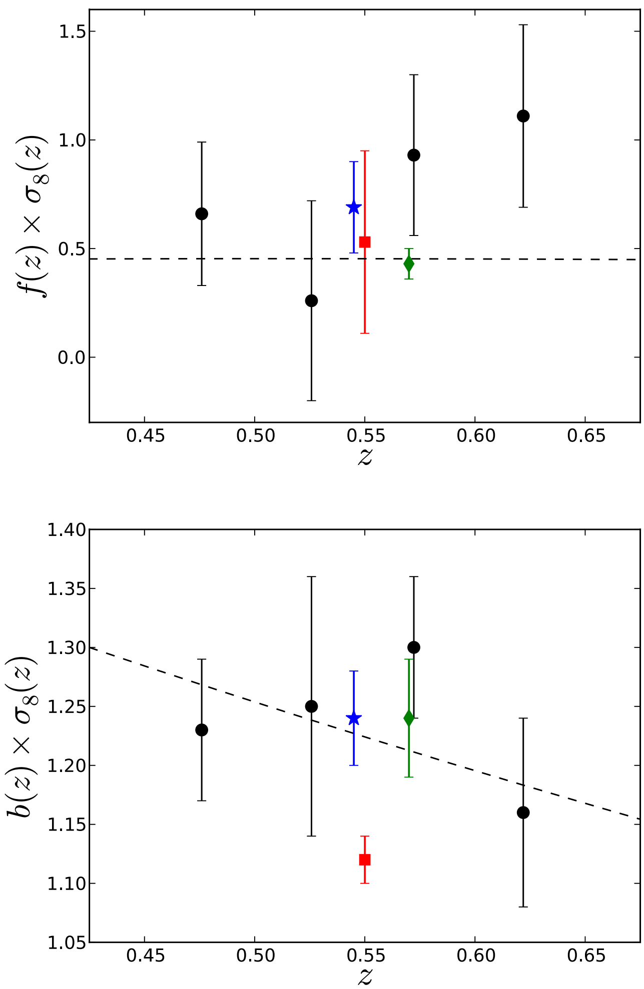

Figure 4. Best-fitting values for the RSD parameters for the first and third approaches as explained in the text: black bullets assuming different $f\sigma_8$ and $b\sigma_8$ for each shell and blue star assuming a constant $b\sigma_8$ and $f\sigma_8$ for all shells. The red squares are the results from Crocce et al. (2011b) and green diamonds from Reid et al. (2012). The dashed lines are the expected theoretical values with $\sigma_8 = 0.8$ and $b = 2$.

Recently, Reid et al. (2012) reported the result for RSD parameters using BOSS DR9 spectroscopic data, which is a subset of the LGs we are analysing. They found $b\sigma_8 = 1.24 \pm 0.05$ and $f\sigma_8 = 0.43 \pm 0.07$ at an effective redshift $z = 0.57$ (their results are shown in Fig. 4 as a green diamond). The $b\sigma_8$ agrees quite well with our results for all approaches. When assuming a constant $f\sigma_8$ for all shells, we find $f\sigma_8 = 0.72 \pm 0.22$ as our best-fitting value, which agrees with Reid et al. (2012) at 1.5σ. For a better comparison with the Reid et al. (2012) results, we analyse the results for our third method, in which case we find $b\sigma_8 = 1.24 \pm 0.04$ and $f\sigma_8 = 0.69 \pm 0.21$ (both results are displayed in Fig. 4 as a blue star); in this case the bias is again consistent, but the velocity growth rate still agrees at the 1.5σ level. Ross et al. (2011b) showed that the highest redshift shell is most likely to be affected by systematic uncertainties, so we performed this last analysis without the last shell, with results $b\sigma_8 = 1.26 \pm 0.04$ and $f\sigma_8 = 0.64 \pm 0.23$, and in this case our results agree with Reid et al. (2012) at 1σ.

In a previous study, Ross et al. (2011a) showed the impact of the assumed cosmology upon the RSD parameters using ACF. They found that changing Ω_m from 0.25 to 0.30 produces a significant effect on $f(z)\sigma_8(z)$ result. The difference between *WMAP*7 and *Planck* results (Ade et al. 2013), for a ΛCDM cosmology, is most pronounced in Ω_m, which increases by ∼10 per cent. Therefore the RSD is affected when assuming *WMAP*7 or *Planck* cosmologies. We re-analysed the data with *Planck* cosmology for the case of constant $f\sigma_8$ and $b\sigma_8$ in all four shells and found that $f\sigma_8$ increases by 33 per cent in comparison to *WMAP*7 cosmology, whereas $b\sigma_8$ does not change significantly, in agreement with Ross et al. (2011a).

In order to check the impact of the assumed cosmology on the covariance matrix we have also performed the fits with a different cosmology, varying Ω_m, Ω_b, h, within the *WMAP*7 allowed values. We found that the best-fitting results and the corresponding χ^2 do not change significantly, with a difference at the sub-per cent level. Therefore we are confident that the approximation of keeping the theoretical covariance matrix fixed at a given cosmology does not bias our results significantly.

We also performed the analysis with only the diagonal errors, in angle and redshift, to check the impact of the covariance matrix on the results. The results for $f\sigma_8$ and its error are affected in a significant manner. The errors are typically four times smaller with respect to the errors with the full covariance matrix and the χ^2 are much higher for all shells. This demonstrates, as expected, that it is crucial to apply the full covariance matrix in the ACF analysis.

6 COSMOLOGICAL PARAMETERS

6.1 PLG analysis

In this section we apply the so-called PLG method (Sánchez et al. 2011) to extract the baryonic acoustic scale in the four redshift bins under analysis. The ACF is fitted around the BAO peak by a function of the form

$$\omega(\theta) = A + B\theta^{\gamma} + C\mathrm{e}^{\frac{-(\theta-\theta_{\rm plg})^2}{2\sigma}}, \quad (22)$$

with six free parameters (A, B, C, γ, σ, $\theta_{\rm plg}$).

We modify the PLG method by imposing some priors in the width of the BAO peak σ. The width of the BAO peak is defined by three factors: silk damping; adiabatic broadening of the acoustic oscillation and correlations of the initial perturbations. In configuration space, this correspond to ≈10 per cent of the BAO scale. Therefore we fix the width of the Gaussian to be proportional to 10 per cent of the BAO scale at a given redshift. We keep as free parameter the proportionality constant p between the width and the mean of the peak, assumed to be independent of redshift. Therefore, from the original 24 free parameters, six for each shell, we have now five free parameters per redshift shell (20 in total, keeping σ fixed), plus one extra free parameter p, related to the width of the peak by

$$\sigma = 0.1\, p\, \theta_{\rm plg}. \quad (23)$$

If we do not impose priors in σ, the PLG method can give unphysical results due to the noisy nature of the ACF measurement. For instance, in the second panel from top to bottom of Fig. 5, a wide peak can be seen in the data around ≈3°.6, but with some decrease of the amplitude at the mean (consistent with noise), producing two peaks: one around 3°.2 and the other around 4°.2. The basic PLG method is not capable of solving this kind of structure, and for this reason we impose the prior discussed above.

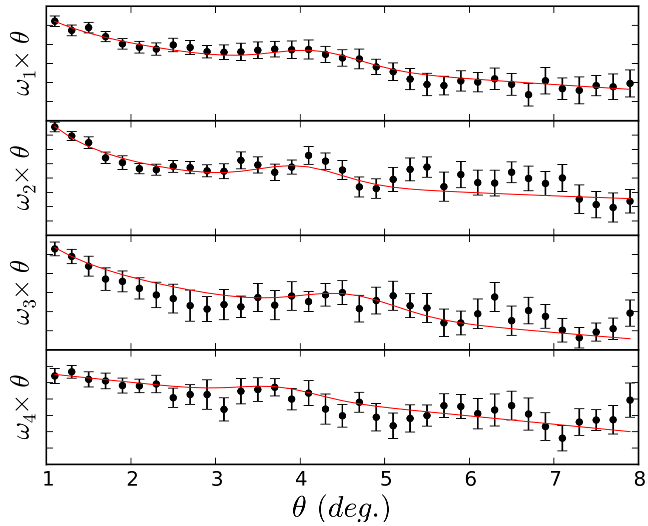

Figure 5. PLG fit (red line) using priors in the width of the Gaussian, to the four ACF (black dots) simultaneously using the full covariance matrix with correlations between redshift shells. We do not display the ACF values for clarity. The redshift shells are arranged from top to bottom with increasing redshift. We use this result as the best case.

The mean of the Gaussian $\theta_{\rm plg}$ is associated with the true angular acoustic scale at redshift z, $\theta_{\rm BAO}(z)$, through a correction $\lambda(z, \Delta z)$ that is independent of cosmology and only depends on redshift and redshift bin width:

$$\theta_{\rm BAO}(z) = \lambda(z, \Delta z)\theta_{\rm plg}. \quad (24)$$

The parametrization of the function $\lambda(z, \Delta z)$ is described in Sánchez et al. (2011), where it is shown that this function does not vary significantly (sub-per cent level) for 14 different cosmologies.

In order to find Δz, one has to face a small difficulty. In a photometric analysis, one defines the top-hat bin width as the difference between the photo-z limits, which does not correspond to the true redshift bin width, due to the smearing by the photo-z error. Therefore, we need to correct the actual top-hat photo-z bin width to obtain the true bin width Δz. In our case, since we have the redshift selection function for each redshift bin, we can estimate the true redshift bin width for each redshift bin from the relation (Simpson et al. 2009)

$$\Delta z = \sqrt{12}\,\sigma_z, \quad (25)$$

where σ_z is the dispersion of the selection function at the given redshift bin. In our analysis, we obtain a true bin width for each bin given by $\Delta z^1_{\rm true} = 0.101$, $\Delta z^2_{\rm true} = 0.130$, $\Delta z^3_{\rm true} = 0.158$ and $\Delta z^4_{\rm true} = 0.185$.

These measurements can then be used to constrain the angular diameter distance as a function of redshift, related by

$$\theta_{\rm BAO}(z) = \frac{r_{\rm s}}{D_{\rm A}(z)}, \quad (26)$$

extracted from the ACF, where $r_{\rm s}$ is the baryonic acoustic scale at decoupling and $D_{\rm A}(z)$ is the angular diameter distance at redshift z.

The four redshift bins are fitted together considering the covariance matrix between redshift shells introduced in Section 3 using the MINUIT library (James & Roos 1975). In total, there are 21 free parameters, with a number of 140 data points and hence 119 degrees of freedom. In Fig. 5, the fit results are shown on top of the

Table 3. PLG fit results for the four redshift bins imposing priors in the width of the BAO peak. The overall quality of the fit is $\chi^2/\mathrm{dof} = 0.96$. θ_{BAO} is obtained after correcting from projection effects (equation 24), and its error accounts for both statistical and systematic errors. The signal-to-noise ratio (S/N) is giving as the strength of the Gaussian divided by its error (in our parametrization, parameter C).

Redshift shell	θ_{plg} (°)	θ_{BAO} (°)	S/N
$0.45 \le z_{\mathrm{p}} \le 0.50$	4.13 ± 0.19	4.48 ± 0.29	2.6
$0.50 \le z_{\mathrm{p}} \le 0.55$	3.93 ± 0.20	4.28 ± 0.29	2.5
$0.55 \le z_{\mathrm{p}} \le 0.60$	4.49 ± 0.31	4.90 ± 0.39	2.0
$0.60 \le z_{\mathrm{p}} \le 0.65$	3.68 ± 0.23	4.01 ± 0.30	1.3

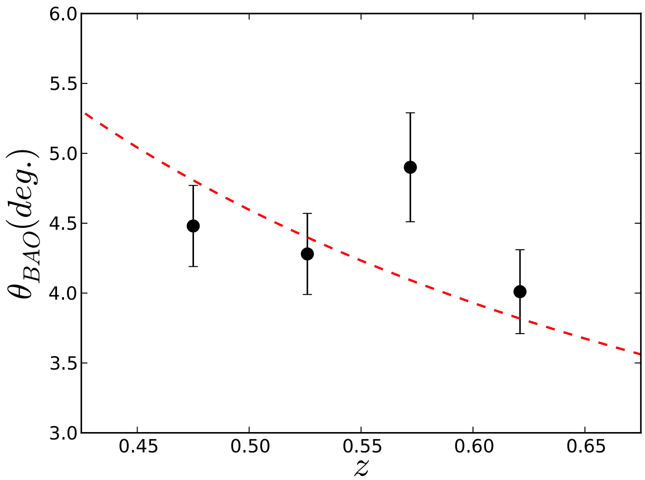

Figure 6. θ_{BAO} as a function of z for the CMASS catalogue. The dashed line is given by the best-fitting cosmology, when the θ_{BAO} measured in the CMB is also used. The best-fitting cosmology is $\Omega_{\mathrm{m}} = 0.249 \pm 0.031$, $w = -0.885 \pm 0.145$, fixing the other parameters to $h = 0.71$ and $\Omega_{\mathrm{b}} = 0.0449$.

measured ACF for the four redshift bins and in Table 3 we display the main values of the fit. The best-fitting value for the proportionality constant is $p = 1.28$, resulting that the width of the acoustic peak is 12.8 per cent the scale of the peak, common to all redshift bins and in agreement with what is expected from theory.

After correcting from projection effects (using the true redshift bin width), we obtain θ_{BAO} for each redshift bin, as shown in Table 3. Errors in $\theta_{\mathrm{BAO}}(z)$ have two main contributions: the statistical error coming from the fit plus an intrinsic error due to the variance introduced by the photometric redshift uncertainty, estimated to be around 5 per cent for a SDSS-like survey (details are found in Carnero et al. 2012). The combined errors are presented in Table 3.

In Fig. 6 the evolution of θ_{BAO} as a function of redshift is shown for our analysis, together with the best-fitting value stated below, when the θ_{BAO} measured in the cosmic microwave background (CMB) is also used. Errors are given as the diagonal term in the full covariance matrix of the parameters for the four redshift shells (statistical plus systematic error).

To find the best-fitting cosmology we parametrize r_{s} as a function of cosmological parameters using the analytical approximation given in Eisenstein & Hu (1998). We then minimize the χ^2 statistics using the four BAO measurements together with the BAO measurement at decoupling measured by *WMAP*7, with $\theta_{\mathrm{BAO}}(z = 1091) = 0^{\circ}.5952 \pm 0^{\circ}.0016$. The best-fitting cosmology for free parameters Ω_{m} and w, fixing the other parameters to $h = 0.71$ and $\Omega_{\mathrm{b}} = 0.0449$, is $\Omega_{\mathrm{m}} = 0.249 \pm 0.031$, $w = -0.885 \pm 0.145$. If we instead use only the DR8 measurements in the (Ω_{m}, w) space, there are not enough degrees of freedom and the cosmology is poorly constrained. Therefore, we fit only Ω_{m} for a ΛCDM model, with a best-fitting result of $\Omega_{\mathrm{m}} = 0.231 \pm 0.079$.

Throughout the analysis we have fixed the effective number of neutrino species to $N_{\mathrm{eff}} = 4.34$, the central value of the result found by *WMAP*7 data in combination with BAO and H_0 priors (Komatsu et al. 2011), which deviates from what is expected in the standard model of particle physics ($N_{\mathrm{eff}} = 3.04$). In order to test the effect of N_{eff} on the cosmological constraints, we find the best-fitting value to Ω_{m} using the BAO measurements from DR8 alone, with $N_{\mathrm{eff}} = 3.26$, obtained in *WMAP*9 (Hinshaw et al. 2012). In this case, the best fit is $\Omega_{\mathrm{m}} = 0.292 \pm 0.090$, ~25 per cent higher than with *WMAP*7 N_{eff}. This result shows that the effective number of neutrino species is an important parameter in the analysis of the BAO if we use it as a standard ruler, and its uncertainty will need to be considered in future analysis.

In order to compare our results with previous measurements, we use the results from Seo et al. (2012), where the BAO position for the same data was obtained from the angular power spectrum with a different methodology and stacked the C_l for each shell together to give a single angular distance measurement at $z = 0.54$. They measured the deviation of the best-fitting cosmology with reference to a fiducial model with $\Omega_{\mathrm{m}} = 0.274$, $w = -1$, $\Omega_{\mathrm{b}} = 0.049$, $h = 0.7$, parametrized by

$$\alpha = D_{\mathrm{A}}(z)/D_{\mathrm{A}}(z)_{\mathrm{fiducial}}. \tag{27}$$

The results found by Seo et al. (2012) was $\alpha = 1.066 \pm 0.047$, after marginalizing over the other cosmological parameters. Our parametrization is different, and we did not calculate a stacked ACF from the four redshift bins. Nonetheless, we can also measure the deviation from the same fiducial cosmology and obtain a value for α using the values obtained with the PLG method. In this case we do not use the BAO measurement from *WMAP*7. Without marginalizing, and using the best-fitting cosmology, we obtain a value of $\alpha = 1.028 \pm 0.035$. This value is roughly at 1σ from the value of Seo et al. (2012). The error is smaller in our case because we have not marginalized over the other parameters. We note that the DR9 BOSS study (Anderson et al. 2013) found that 1σ differences between the BAO position recovered from the power spectrum and that recovered from the correlation function were not unusual.

6.2 Full shape analysis

In this section we apply the full shape information of the ACF to constrain a subset of cosmological parameters, namely Ω_{m}, $f_{\mathrm{b}} = \Omega_{\mathrm{b}}/\Omega_{\mathrm{m}}$, σ_8 and bias. Following Blake et al. (2007) and Thomas et al. (2010), we assume the bias to be scale independent and constant within each shell. The other cosmological parameters are held fixed at the *WMAP*7 values given previously. The χ^2 function was constructed as discussed in Section 3 and we used the COSMOMC package (Lewis & Bridle 2002) to search the parameter space, with no priors imposed in any of the free parameters.

First we consider the behaviour of the parameters σ_8 and bias b. These two parameters are highly degenerate, making it difficult to constrain them separately (Okumura et al. 2008). Therefore we show the constraint of their product for each redshift combined: $\sigma_8 b_1 = 1.46 \pm 0.09$, $\sigma_8 b_2 = 1.49 \pm 0.10$, $\sigma_8 b_3 = 1.63 \pm 0.12$ and $\sigma_8 b_4 = 1.51 \pm 0.15$. In order to compare with the previous results

Table 4. Best-fitting values from the full-shape ACF analysis for Ω_m and $f_b = \Omega_b/\Omega_m$, after marginalizing over σ_8 and bias, with all other parameters being kept fixed at the *WMAP*7 cosmology as stated in the text.

Redshift shell	Ω_m	f_b	χ^2/dof
$0.45 \le z_p \le 0.50$	0.29 ± 0.04	0.25 ± 0.04	0.65
$0.50 \le z_p \le 0.55$	0.37 ± 0.05	0.14 ± 0.04	1.49
$0.55 \le z_p \le 0.60$	0.25 ± 0.04	0.13 ± 0.04	0.79
$0.60 \le z_p \le 0.65$	0.23 ± 0.04	0.23 ± 0.06	0.62
All shells combined	0.280 ± 0.022	0.211 ± 0.027	1.05

from the RSD analysis (see Section 5) we assume $\sigma_8 = 0.801$ as before: $b_1 = 1.82 \pm 0.12$, $b_2 = 1.86 \pm 0.13$, $b_3 = 2.03 \pm 0.15$ and $b_4 = 1.89 \pm 0.17$. Although the results from the full shape analysis are typically 5 per cent lower, they all agree at the 1σ level.

We now focus our attention on other parameters in our cosmological analysis, namely Ω_m and f_b. First we perform the analysis for each shell independently in order to check the dispersion of the best-fitting values. In this case we have four free parameters. In Table 4 we show our results. Both parameters vary appreciably among different redshift shells, but they all agree within 2σ. Even though the dispersion is non-negligible, the best-fitting values oscillate around the expected results coming from *WMAP*7 namely, $\Omega_m = 0.266$ and $f_b = 0.17$. This result already indicates that the combination of all shells will give results in agreement with *WMAP*7, anticipating the main results of this analysis. When comparing with the analysis from Blake et al. (2007) and Thomas et al. (2010), which used the angular power spectrum, we found that our results are compatible in all shells. Compared to the results of Thomas et al. (2010), the errors on the parameters that we find are smaller, because the area and number of galaxies in our data set are larger.

The analysis for all combined redshift shells also accounts for the correlation among shells. For this analysis we have seven free parameters, the best-fitting results for Ω_m and f_b are displayed in Table 4 and the marginalized probability distribution function and the 2D likelihood contours are shown in Fig. 7 for all parameters analysed. The results are $\Omega_m = 0.280 \pm 0.022$ and $f_b = 0.211 \pm 0.026$ which translates into $\Omega_b = 0.059 \pm 0.008$. The matter density parameter found in our analysis is in good agreement with the value from *WMAP*7, with a difference of 5 per cent. The baryon fraction best fit is higher than *WMAP*7, ~20 per cent, but in agreement within 1σ. In Fig. 8 we show the ACF measurements together with the best-fitting ACF for this analysis. It shows that the model is in good agreement with the measurements and the BAO peak is evident for three redshift shells as already shown in the previous

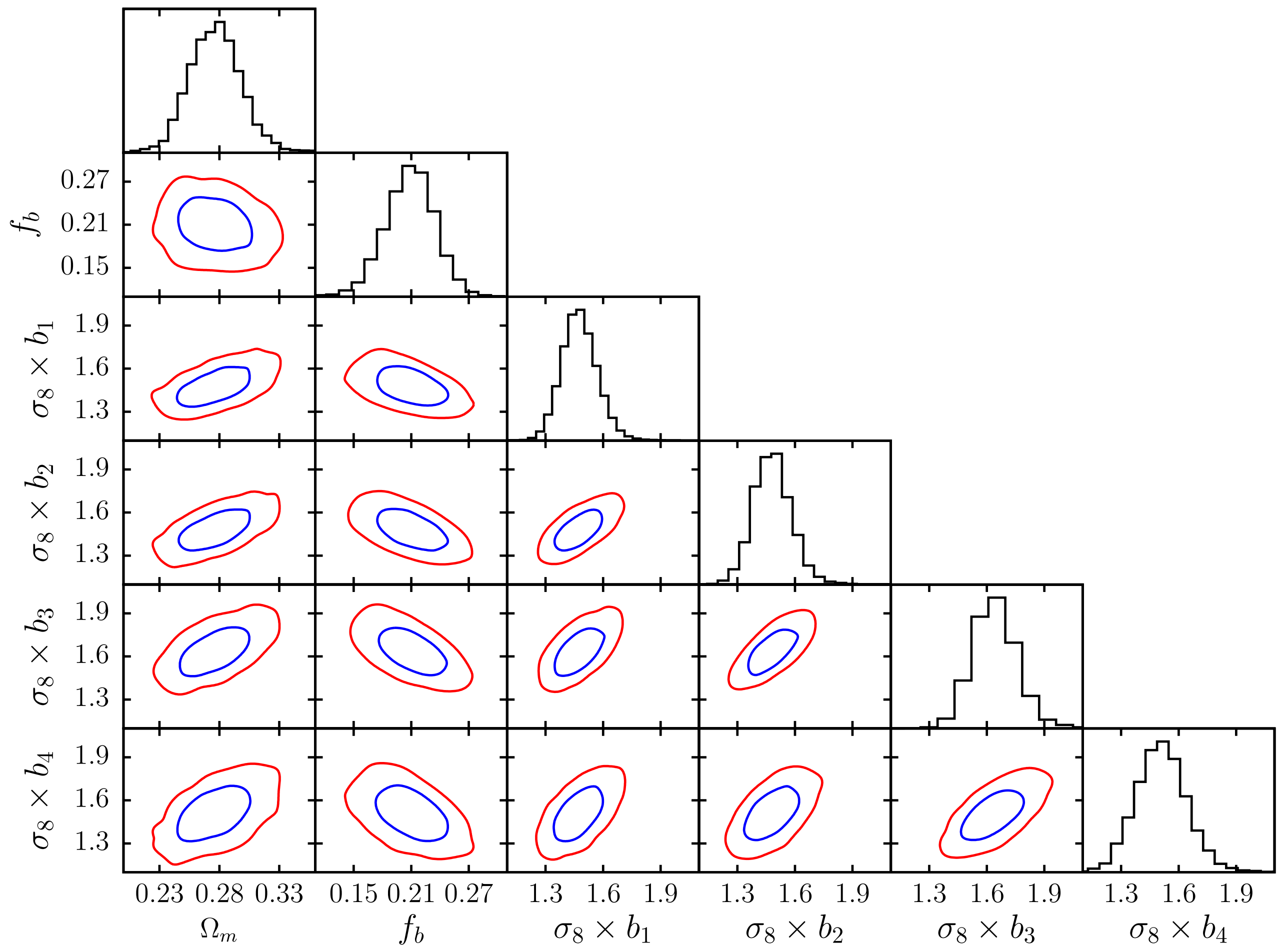

Figure 7. Likelihood contours for (Ω_m, f_b, $\sigma_8 b_1$, $\sigma_8 b_2$, $\sigma_8 b_3$, $\sigma_8 b_4$) with all other parameters being kept fixed in *WMAP*7 cosmology. The diagonal panels display the marginalized likelihood for each one of the six parameters. The other plots show the 1σ and 2σ confidence regions of each pair of parameters, with the other marginalized.

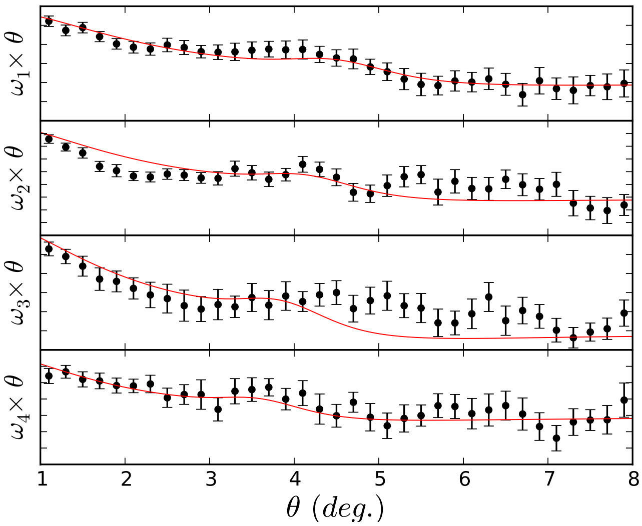

Figure 8. Best-fitting ACF full shape information when combining all shells given in the last line of Table 4 (red line) together with the measurements (black dots). Not only the angular bins are correlated but also the ACF between shell. We do not display the ACF values for clarity. The redshift shells are arranged from top to bottom with increasing redshift.

section. The higher χ^2 for the second shell is evident due to the poor fit at small scales.

As stated in the previous section, the main difference between *WMAP*7 and *Planck* results is $\Omega_{\rm m}$ and the Hubble parameter. The former is ~10 per cent higher with *Planck*'s data and the latter is ~4 per cent lower. As $\Omega_{\rm m}$ is left as a free parameter in our analysis, it is not an issue, but h is fixed. As shown in Blake et al. (2007) the major effect of changing h is in the $\Omega_{\rm m}$ best fit. Because the clustering characteristics are driven mostly by the combination $\Omega_{\rm m}h$, lowering h implies in the increase of $\Omega_{\rm m}$. Since our best fit with *WMAP*7 Hubble parameter is $\Omega_{\rm m} = 0.280$, if we instead use $h = 0.68$, as found by *Planck*, we would have found a higher value, in better agreement with $\Omega_{\rm m}$ quoted by *Planck*.

As an additional cross-check of the results in this section, we have repeated the analysis above using a completely independent set of codes, both for the estimation of the theoretical ACF as well as for the Monte Carlo sampling. We coupled the independent ACF code to the EMCEE sampler (Foreman-Mackey et al. 2013) and repeated all the calculations. We find that the results obtained from CosmoMC and EMCEE are in most cases nearly identical and in all cases consistent with each other within 1σ errors.

The quoted errors of 8 per cent for $\Omega_{\rm m}$ and 12 per cent for $f_{\rm b}$ are underestimated since they do not take into account the marginalization of the other parameters. For more realistic errors, we should have varied all parameters, including the Hubble parameter h, spectral index $n_{\rm s}$ and the dark energy equation of state parameter w, and marginalized over them. Unfortunately the statistical significance of our data set alone is not sufficient to obtain useful constraints. Combining our results with a CMB likelihood, e.g. from *WMAP* or *Planck*, would probably allow for a more complete analysis and for better constraints due to the complementarity of these probes (see e.g. Ho et al. 2012).

Nonetheless, our results point out that the methods applied to extract information from measurements of ACF in configuration space are able to yield competitive cosmological constraints. This indicates that these methods will be even more useful when applied to future data sets with greater constraining power. The combination with other probes of large-scale structure and CMB should provide additional consistency checks and even better constraints.

7 SUMMARY AND CONCLUSIONS

We have analysed the large-scale ACF of luminous galaxies from the SDSS-DR8 photometric data. The ACF was measured in four photo-z shells with the novel approach develop by Ross et al. (2011a) and Ho et al. (2012), which incorporates systematics effects and was able to remove the excess of power at large scales as reported by previous studies (Sawangwit et al. 2011; Thomas et al. 2011).

We have performed three different analyses using the measured ACFs: RSD; BAO detection using the PLG method and a cosmological analysis with the ACF full shape information. The latter represents, to the best of our knowledge, the first cosmological analysis performed with the ACF in configuration space. All three analyses accounted for the correlation between redshift shells and effects of photo-z errors encoded in the selection function. Our main results are the following.

(i) Within the redshift-space parameters best fit and assuming $\sigma_8 = 0.801$, we found that the bias parameters are in good agreement with other DR8 measurements, such as those by Ho et al. (2012).

(ii) When allowing for arbitrary values of $f\sigma_8$ in each redshift shell, the RSD parameters vary appreciably around the expected value from ΛCDM cosmology, in agreement with the findings of Crocce et al. (2011b).

(iii) When assuming constant RSD parameters over the survey range we found $b\sigma_8 = 1.24 \pm 0.04$ and $f\sigma_8 = 0.69 \pm 0.21$. The bias parameter agrees quite well with BOSS DR9 measurements (Reid et al. 2012), and the growth rate agrees within 1.5σ.

(iv) We extracted the position of the BAO peak using the PLG parametrization for all four shells, and combined these measurements with the BAO peak in the CMB data from *WMAP*7. We obtained cosmological constraints of $\Omega_{\rm m} = 0.249 \pm 0.031$ and $w = -0.885 \pm 0.145$. For a ΛCDM model, and using only our own ACF measurements, we obtained $\Omega_{\rm m} = 0.231 \pm 0.079$ with other parameters fixed at our fiducial cosmology.

(v) Within the ACF full shape analysis we constrained $\Omega_{\rm m}$ and $f_{\rm b}$ for each redshift shell independently, and found that the best-fitting values oscillate around the *WMAP*7 values, but are all within 2σ.

(vi) When analysing all shells combined, with the full covariance matrix accounting for the redshift correlations, the best-fitting values were $\Omega_{\rm m} = 0.280 \pm 0.022$ and $f_{\rm b} = 0.211 \pm 0.026$ in reasonable agreement with *WMAP*7.

(vii) Both analysis performed in this work to constrain cosmology, namely the BAO peak and full shape information, agree in the $\Omega_{\rm m}$ best-fitting values, showing that both methods are consistent with each other.

We have shown that the ACF estimated from photometric data can be efficiently applied to constrain cosmological parameters. The ACF results for the photometric DR8 data are clearly not as competitive as those from the spatial correlation function, which already provides stronger constraints with the BOSS DR9 data (Anderson et al. 2012; Sánchez et al. 2012). Nonetheless, our results are encouraging for future photometric surveys, such as the DES, Panoramic Survey Telescope and Rapid Response System (PanSTARRS) and LSST, which will probe larger redshifts and measure significantly more galaxies. In this case, the ACF measurements have the potential to accurately constrain a larger number of cosmological parameters (Sobreira et al. 2011), allowing for extra consistency checks with other independent probes.

ACKNOWLEDGEMENTS

We thank the anonymous referee for useful comments on the manuscript. We thank Joe Zuntz for useful discussions on MCMC codes and Shirley Ho for comments on the draft paper. FdS would like to thank Mariana Penna-Lima and Sandro Vitenti for valuable interactions.

AC and FS acknowledge financial support from CNPq (PCI-D grants 311876/2011-0 and 303186/2011-9, respectively, both associated with the PCI/MCT/ON Program). HOC is supported by CNPq. ML and RR are partially supported by FAPESP and CNPq.

This research was carried out with the support of the Laboratório Interinstitucional de e-Astronomia (LIneA) operated jointly by the Centro Brasileiro de Pesquisas Físicas (CBPF), the Laboratório Nacional de Computação Científica (LNCC) and the Observatório Nacional (ON), and funded by the Ministério de Ciência e Tecnologia (MCT).

Funding for SDSS-III has been provided by the Alfred P. Sloan Foundation, the Participating Institutions, the National Science Foundation and the US Department of Energy Office of Science. The SDSS-III web site is http://www.sdss3.org/

SDSS-III is managed by the Astrophysical Research Consortium for the Participating Institutions of the SDSS-III Collaboration including the University of Arizona, the Brazilian Participation Group, Brookhaven National Laboratory, University of Cambridge, Carnegie Mellon University, University of Florida, the French Participation Group, the German Participation Group, the Instituto de Astrofísica de Canarias, the Michigan State/Notre Dame/JINA Participation Group, Johns Hopkins University, Lawrence Berkeley National Laboratory, Max Planck Institute for Astrophysics, New Mexico State University, New York University, Ohio State University, Pennsylvania State University, University of Portsmouth, Princeton University, the Spanish Participation Group, University of Tokyo, University of Utah, Vanderbilt University, University of Virginia, University of Washington and Yale University.

REFERENCES

Abate A. et al., 2012, preprint (arXiv:1211.0310)
Abazajian K. N. et al., 2009, ApJS, 182, 543
Planck Collaboration et al., 2013, preprint (arXiv:1303.5076)
Aihara H. et al., 2011, ApJS, 193, 29
Anderson L. et al., 2012, MNRAS, 427, 3435
Anderson L. et al., 2013, preprint (arXiv:1303.4666)
Blake C., Collister A., Bridle S., Lahav O., 2007, MNRAS, 374, 1527
Blake C. et al., 2011, MNRAS, 418, 1707
Carnero A., Sánchez E., Crocce M., Cabré A., Gaztañaga E., 2012, MNRAS, 419, 1689
Challinor A., Lewis A., 2011, Phys. Rev. D, 84, 043516
Colless M. et al., 2001, MNRAS, 328, 1039
Collister A. A., Lahav O., 2004, PASP, 116, 345
Collister A. et al., 2007, MNRAS, 375, 68
Crocce M., Scoccimarro R., 2008, Phys. Rev. D, 77, 023533
Crocce M., Cabré A., Gaztañaga E., 2011a, MNRAS, 414, 329
Crocce M., Gaztañaga E., Cabré A., Carnero A., Sánchez E., 2011b, MNRAS, 417, 2577
Dawson K. S. et al., 2013, AJ, 145, 10
de Putter R. et al., 2012, ApJ, 761, 12
Eisenstein D. J., Hu W., 1998, ApJ, 496, 605
Finkbeiner D. P. et al., 2004, AJ, 128, 2577
Foreman-Mackey D., Hogg D. W., Lang D., Goodman J., 2013, PASP, 125, 306
Gorski K. M., Hivon E., Banday A. J., Wandelt B. D., Hansen F. K., Reinecke M., Bartelmann M., 2005, ApJ, 622, 759
Hamilton A. J. S., 1992, ApJ, 385, L5
Hinshaw G. et al., 2012, preprint (arXiv:1212.5226)
Ho S. et al., 2012, ApJ, 761, 14
James F., Roos M., 1975, Comput. Phys. Commun., 10, 343
Komatsu E. et al., 2011, ApJS, 192, 18
Lewis A., Bridle S., 2002, Phys. Rev. D, 66, 103511
Matsubara T., 2000, ApJ, 537, L77
Okumura T., Matsubara T., Eisenstein D. J., Kayo I., Hikage C., Szalay A. S., Schneider D. P., 2008, ApJ, 676, 889
Padmanabhan N. et al., 2007, MNRAS, 378, 852
Parkinson D. et al., 2012, Phys. Rev. D, 86, 103518
Percival W. J., Cole S., Eisenstein D. J., Nichol R. C., Peacock J. A., Pope A. C., Szalay A. S., 2007, MNRAS, 381, 1053
Press W. H., Flannery B. P., Teukolsky S. A., 1986, Numerical Recipes. The Art of Scientific Computing. Cambridge Univ. Press, Cambridge
Reid B. A. et al., 2012, MNRAS, 426, 2719
Ross A. J., Percival W. J., Crocce M., Cabré A., Gaztañaga E., 2011a, MNRAS, 415, 2193
Ross A. J. et al., 2011b, MNRAS, 417, 1350
Sánchez E. et al., 2011, MNRAS, 411, 277
Sánchez A. G. et al., 2012, MNRAS, 425, 415
Sawangwit U., Shanks T., Abdalla F. B., Cannon R. D., Croom S. M., Edge A. C., Ross N. P., Wake D. A., 2011, MNRAS, 416, 3033
Schlafly E. F., Finkbeiner D. P., 2011, ApJ, 737, 103
Seo H.-J. et al., 2012, ApJ, 761, 13
Simpson F., Peacock J. A., Simon P., 2009, Phys. Rev. D, 79, 063508
Sobreira F., de Simoni F., Rosenfeld R., da Costa L. A. N., Maia M. A. G., Makler M., 2011, Phys. Rev. D, 84, 103001
The Dark Energy Survey Collaboration, 2005, preprint (astro-ph/0510346)
Thomas S. A., Abdalla F. B., Lahav O., 2010, preprint (arXiv:1011.2448)
Thomas S. A., Abdalla F. B., Lahav O., 2011, Phys. Rev. Lett., 106, 241301
White M. et al., 2011, ApJ, 728, 126
York D. G. et al., 2000, AJ, 120, 1579

This paper has been typeset from a TEX/LATEX file prepared by the author.